Scientific Research Publishing

Open Journal of Civil Engineering, 2025, 15(4), 741-754
https://www.scirp.org/journal/ojce
ISSN Online: 2164-3172
ISSN Print: 2164-3164

Numerical Analysis and Review of Detailing Practices of Slabless Staircase

Emmanuel Oladipupo Oyakojo

Lyles School of Civil and Construction Engineering, Purdue University, West Lafayette, Indiana, USA
Email: eoyakojo@purdue.edu

How to cite this paper: Oyakojo, E.O. (2025) Numerical Analysis and Review of Detailing Practices of Slabless Staircase. *Open Journal of Civil Engineering*, **15**, 741-754.
https://doi.org/10.4236/ojce.2025.154040

Received: October 14, 2025
Accepted: November 15, 2025
Published: November 18, 2025

Abstract

The analysis and detailing of the slabless staircase represent a critical factor in their limited commercial and residential usage compared to the waist slab staircase, despite their architectural attractiveness. Literature in the past and present has provided analysis and detailing of slabless staircase based on analytical and engineering judgment. Extensive knowledge of its behavior in terms of failure modes, crack patterns, and stress flow is necessary to evaluate the efficacy of these detailing practices. This paper presents the results of corresponding numerical investigations on four reinforced concrete detailing practices for single-flight slabless staircases. The study is conducted using the 3D Finite Element (FE) approach, where the constitutive law of concrete is based on the microplane model with relaxed kinematic constraints. The load was applied in a downward monotonic displacement control manner at the mid-span of each model, and the analysis results are evaluated in terms of load-displacement behavior, failure load, and failure mode. The numerical investigations provide a deeper insight into the detailed behavior of reinforced concrete slabless stairs through the visualization of crack patterns, stress flows, and strain development in concrete. The results show that slabless detailing options with stirrups formed as chains of links along the longitudinal direction serve as a conservative approach compared to other options that could serve the same purpose.

Keywords

Slabless Staircase, Waist Staircase, Finite Element Method, Slabless Detailing

1. Introduction

A slabless staircase, also known as a sawtooth staircase, is a series of stairs that has its tread and riser as its structural elements. Conversely, the waist slab staircase relies on its waist under the step to resist the load on it. The slabless staircase's

attractive architectural effects ensure its preference over a waist staircase, albeit its cumbersome formwork construction and uneconomical detailing practices.

The complexity of the slabless stairs geometry, which mimics the configuration of a folded plate, complicates its analysis, necessitating the use of an accelerated computer-aided modified Fourier series Jiang *et al.* [1]. Consequently, researchers over the years have provided comparative, simplified analytical models and empirical detailing practices on slabless stairs.

Saenz and Martins [2] provided a detailed description of slabless stairs, in which it was opined that strirrups be laid along the longitudinal direction of the stairs to form a chain-like configuration. It was suggested that the rebar arrangement enhances the development of the bar, provides confinement, and therefore ensures the ductility of the system. Similarly, Cusens [3] recommended using closed-loop rebars and planar straight rebars to cater for the haunches at the joints where stress concentration is expected.

In recent years, scientists have investigated different configurations of closed-loop rebars with and without planar reinforcement for detailing slabless stairs.

Özbek *et al.* [4] conducted experiments on slabless staircases with different arrangements of closed-loop rebars with or without planar longitudinal rebars. The design matrix for this experiment is the variation of the tread and riser thickness. Four evenly spaced hydraulics were used to apply a perpendicular monotonic loading to the tread plane. It was reported that planar reinforcement significantly improved the stiffness and strength of the system while preventing the debonding of the rebars.

Interestingly, Sabeeh *et al.* [5] investigated numerically the flexural behavior of slabless stairs with different detailing of closed loops, while additional rebars were installed to form a series of strut and tie configurations. It was reported that the triangular configuration at the mid-span of the specimen provided a significant increase in the load capacity. However, its ductility index decreased slightly when compared to specimens without triangular configurations.

To better understand the behavior of a slabless staircase, specifically due to the shear concentration expected at the tread-riser joints, it is expedient to use numerical approaches, with Finite Element (FE) being the most prominent one. The FE approach is a crucial tool for gaining local insight into stresses, strains, and deformations in concrete and steel. Furthermore, it serves as an alternative to costly experiments in designing and constructing the setup of the slabless staircase.

All of the studies in the literature were on closed-loop details in slabless stairs. None of the aforementioned studies compared other detailing practices available in practice with closed-loop details. In simple terms, no research has been carried out on other detailing practices besides closed-loop detailing practices of slabless stairs.

This study aims to investigate numerically and review the detailing practices available for slabless staircases through the visualization of crack pattern, stress

flow, and strain development, while comparing the failure loads (obtained from the specimens under review) with the ultimate allowable load in relevant codes [6]-[8], using a staircase in a school as a case study.

Research Significance

All studies in the literature have focused on closed-loop detailing practice for slabless staircase, where the configuration forms a zigzag chain along the length of the stairs. No experimental or numerical investigations have been reported, at the point of writing this paper, on other detailing practices available. This paper will employ a numerical approach to investigate the failure modes and crack patterns of three other detailing practices and evaluate the efficacy of their reinforcement arrangements in comparison to the closed-loop detailing configuration.

2. FE Modeling Approach and Validation

2.1. Constitutive Law for Concrete

The Finite Element program MASA was developed at the Institute of Construction Materials, University of Stuttgart. It was created for the two- and three-dimensional nonlinear analysis of structural components made of quasi-brittle materials, such as concrete. The code uses a microplane model with a relaxed kinematic constraint as the constitutive law of concrete. The microplanes represent weak planes between the aggregates in concrete, on which stress-strain relationships are defined Ožbolt *et al.* [9].

The microplane model is based on the concept of relaxed kinematic constraints, and each microplane is defined by its normal vector, as shown in **Figure 1**, which acts as a weak layer between the aggregates and the cement matrix.

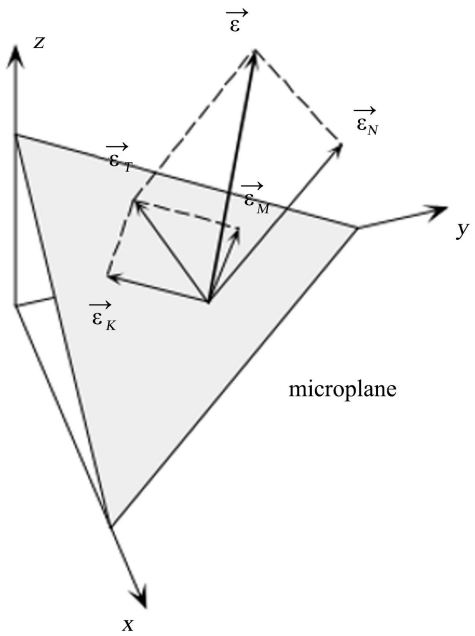

Figure 1. Microplane strain components.

It is essential to note that the kinematic constraint is a hypothetical concept that defines the microplane strains as the direct decomposed components of the macroscopic strain tensor. Consequently, the total macroscopic strain tensor is decomposed into shear and normal components on a predefined microplane.

Furthermore, decomposing the normal strain tensor results in volumetric and deviator components in Equation (2.1) and is shown graphically in Figure 2.

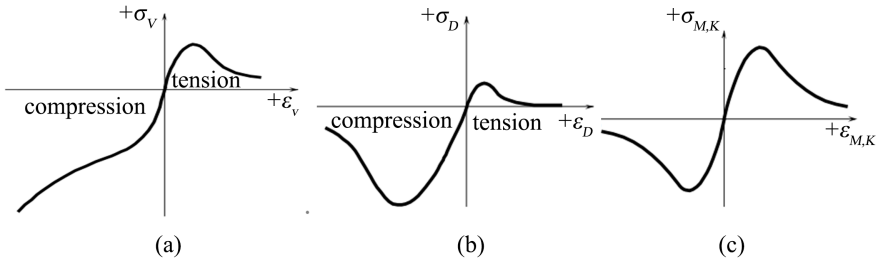

Figure 2. Schematic plot of Microplane stress-strain relationships (a) Volumetric component σ_V, (b) Deviatoric component σ_D, (c) Both shear stress-strain components.

$$\sigma_V = F_V\left(\varepsilon_{v,eff}\right);\ \sigma_D = F_D\left(\varepsilon_{D,eff}\right);\ \sigma_{Tr} = F_{Tr}\left(\varepsilon_{Tr,eff}\right) \tag{2.1}$$

where F_V, F_D and F_{Tr} are the uniaxial stress-strain relationships for volumetric, deviatoric, and shear components. n_i is the normal vector component, k_i and m_i are the directions of shear components on the microplane, σ_{ij} represents the Kronecker delta, and Ω connotes the surface of the unit radius sphere illustrated in Figure 3.

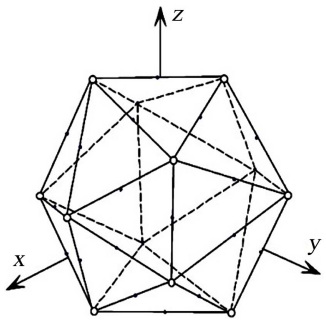

Figure 3. Spatial discretization of unit radius sphere for each integration point. The Figure was taken from Lachinger *et al.* [10].

Moreover, the numerical integration of the established micro-stress components over all microplane orientations on the unit radius sphere delivers the desired macroscopic stress (σ_{ij}) in Equation (2.2). It is expedient that the integration be done incrementally due to the material nonlinearity and path dependency associated with cyclic loading.

$$\sigma_{ij} = \sigma_v\delta_{ij} + \frac{3}{2\pi}\int_\Omega \sigma_N n_i n_j \mathrm{d}\Omega + \frac{3}{2\pi}\int_\Omega \frac{\sigma_{Tr}}{2}\left(n_i\delta_{rj} + n_j\delta_{ri}\right)\mathrm{d}\Omega \tag{2.2}$$

The modelling procedure used in this work has been well-proven to realistically

simulate the behavior of deformed rebars in concrete under various loading conditions by researchers in the past [11]-[14].

2.2. FE Model for Bonded Rebars

Figure 4 depicts Finite Element models of reinforced concrete components consisting of concrete elements (white) discretized into four-node (tetrahedron), and the bonded reinforcement (blue) and contact layer between rebar and concrete are modeled using solid 8-node hexahedral elements.

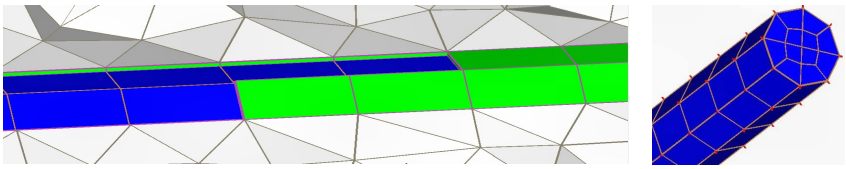

(a) (b)

Figure 4. (a) Finite element meshing of rebar & contact layer (b) Bar elements (in red) protruding from rebar elements.

The contact layer in green (**Figure 4(a)**) is a negligible weak layer that houses the bond bar elements. In addition, the contact layer prevents the transmission of forces between the rebar and concrete elements [11], such that the interface characteristics between concrete and reinforcement are only governed by the bond bar elements.

The slabless stairs components are modeled in full for all the numerical test specimens. With element sizes of components discretized to approximately 15 mm for reinforcement rebars, contact, and concrete elements, where failure mechanisms are expected. Meanwhile, the concrete mesh size increases outward to 25 mm at the edges, where concrete cracks are most likely to occur.

2.2.1. Bond Model

Bar elements imitate the mortar properties between the reinforcement and the concrete. Bar elements protruding from rebar elements in **Figure 4(b)** transfer shear and compression forces using one-dimensional elements from the rebar node and the adjacent concrete node Rao *et al.* [15], which adhere to the bond stress-slip relationship, in **Figure 5** [16].

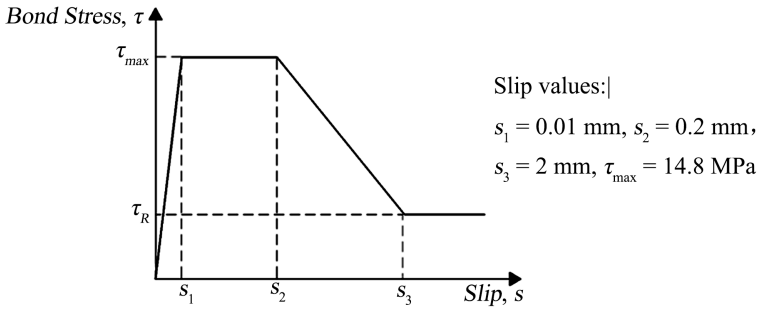

Figure 5. Bond-stress slip curve of 2D bar elements.

In this work, cracks in concrete are visualized using the principal tensile strain, with a strain value of 0.012 corresponding to a crack width of 0.3 mm (see Figure 6). To ensure uniformity throughout this work, this legend will be consistently used.

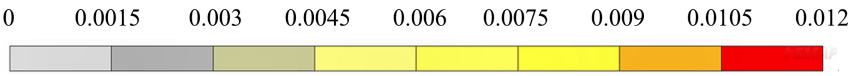

Figure 6. Legend of principal tensile strain.

2.2.2. Constitutive Law for Reinforcement Steel

The uniaxial stress-strain law defines the constitutive law for reinforcement steel. In this paper, a tri-linear stress-strain curve, shown in Figure 7, is characterized by four parameters: 1) Initial Young's modulus. E_0, 2) hardening modulus E_t, 3) yield stress f_y, 4) tensile (compressive) strength f_s. For visualizing stresses along the reinforcement steel length in Femap, the Von Mises stress is used to plot the stresses in the steel.

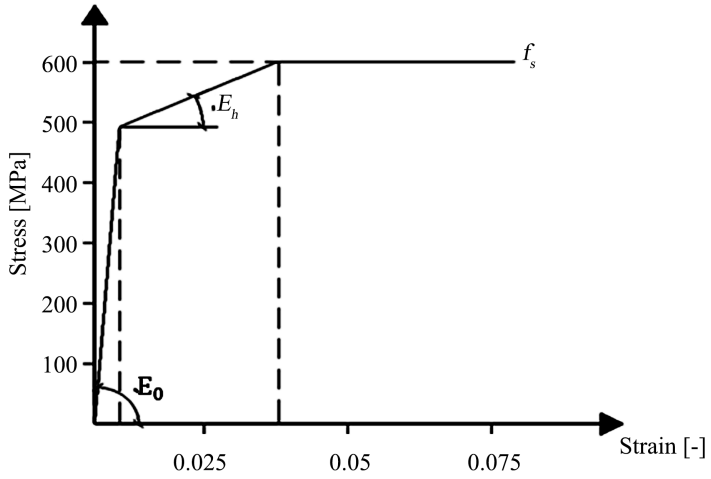

Figure 7. Constitutive stress-strain relationship for reinforcement.

2.3. Material Parameters

As discussed above, the model uses the microplane parameters obtained from microscopic material properties. Consequently, the macroscopic concrete properties utilized for this analysis are the concrete behavior that corresponds to the cylinder compressive strength of concrete; f_c = 24.80 MPa. Interestingly, other concrete material properties are derived from it as follows.

According to Karihaloo [11], the mean concrete strength was calculated.

$$f_t = 0.3 \cdot f_c^{0.67} = 0.3 \cdot \left(24.8\ \mathrm{N/mm^2}\right)^{0.67} = 2.58\ \mathrm{N/mm^2}$$

The fracture energy of the concrete was computed according to [17], assuming a size of 16 mm diameter, where α_f Assumed a value of 7.

$$G_f = \alpha_f f_c^{0.7} = 7 \cdot \left(24.8\ \mathrm{N/mm^2}\right)^{0.7} = 66\ \mathrm{Nm/m^2}$$

The modulus of elasticity of concrete was calculated in line with [6] as:

$$E_c = 4730\sqrt{f_c} = 4730\sqrt{24.8\ \mathrm{N/mm^2}} = 23555\ \mathrm{N/mm^2}$$

Table 1 provides a summary of the mechanical properties of concrete and rebars used for the FE analysis.

Table 1. Mechanical material properties used in the FE analysis.

Property	Concrete	Rebars
Young's Modulus E (GPa)	24	200
Poisson's ratio v [-]	0.18	0.33
Compressive strength f_c'	24.8	-
Tensile strength f_t	2.58	-
Fracture energy G_f [Nmm/mm^2]	0.07	
Yield stress f_y [MPa]	-	595
Ultimate stress f_u [MPa]	-	706

2.4. Description of RC Detailed Cases Analyzed

A typical FE model, showing the boundary conditions and applied load, is illustrated in Figure 8. The concrete elements at and near the supports and under the applied load (regions coloured black) are given linear-elastic stress-strain characteristics to avoid unrealistic local stress concentrations. The load was applied in a downward monotonic displacement control manner, with a 0.2 mm displacement factor, to a total load increment of 100 steps (20 mm).

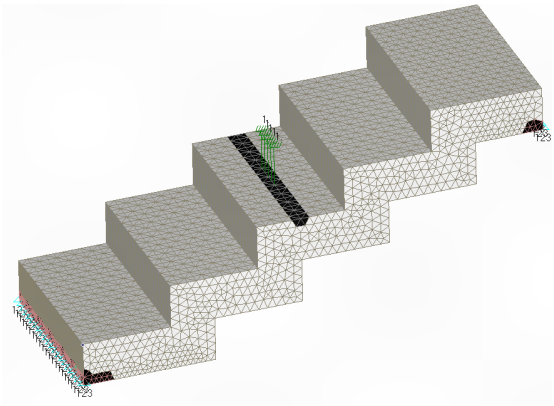

Figure 8. FE mesh of typical specimen.

Table 2 shows schematic drawings of all four (4 Nos.) specimens. The clear stair span of 1650 mm and a width of 600 mm were chosen to reduce the computation time of the analysis. Furthermore, the tread width is 300 mm, while the tread and riser thickness are 150 mm. The tread and riser thickness of 150 mm was chosen to investigate the post-peak behavior of the load-displacement graph, without be-

ing bewildered by excessive deflection, as all specimens were subjected to a monotonic displacement control scheme. All the specimens contained Ø10 mm deformed bars as longitudinal and transverse reinforcement.

Table 2. Reinforcement detailing of specimens cross-section. Units in millimeters.

Specimens Cross-section of Rebar Detailing
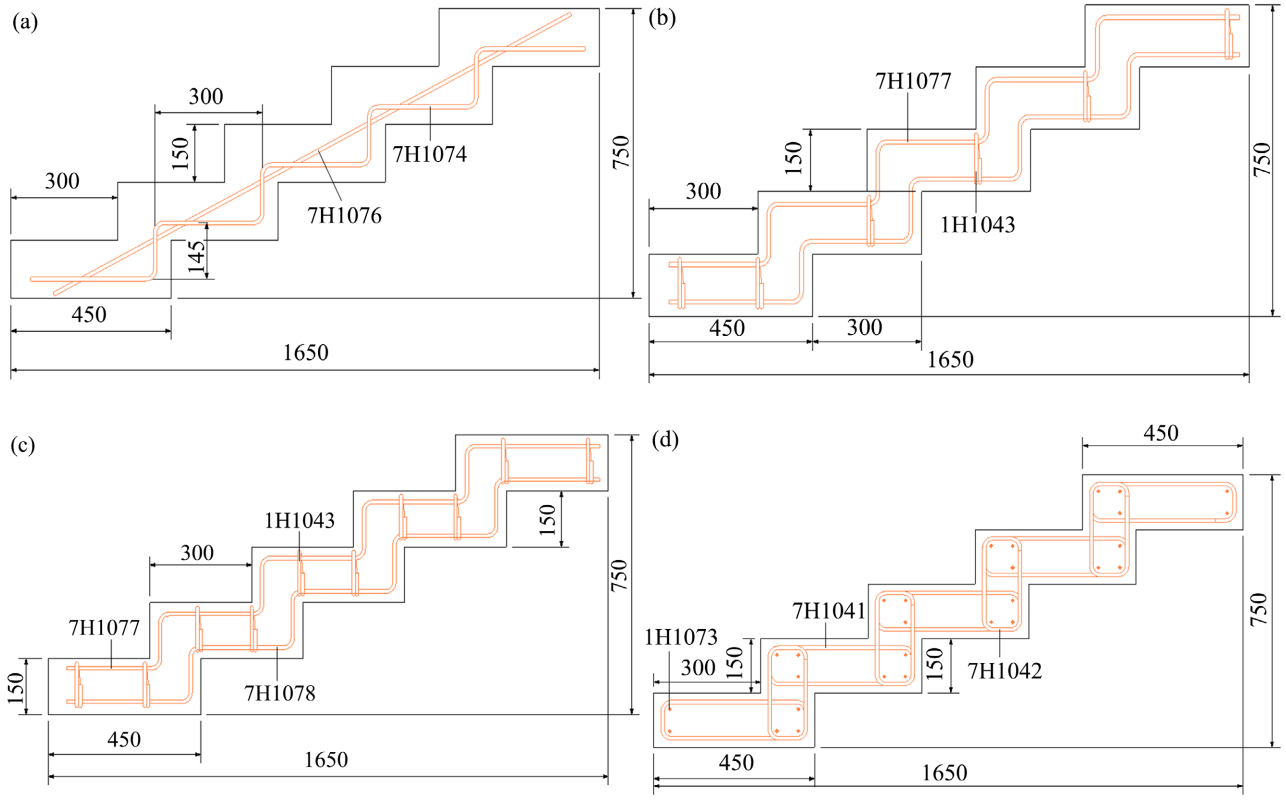

Specimen 1's reinforcement arrangement consists of zigzag planar bars, formed in the shape of stairs, serving as the main rebar, and an adjoining planar straight bar along the length of the staircase. Specimens 2 and 3 have the zigzag planar bars installed at the top and bottom of the staircase layers. While a single transverse closed-loop rebar is provided at each tread section of specimen 2, double transverse closed-loop rebars are installed along the treads for specimen 3. However, closed-loop rebars were placed in the longitudinal direction for specimen 4, and transverse straight bars were placed along the staircase width.

3. Results and Discussion

In this section, the results of the numerical analysis on specimens 1 - 4 are presented and discussed in detail. Furthermore, the failure mechanisms, load-deformation behavior (see **Figure 9**), crack propagation, and strain development will serve as the basis for discussing and comparing all the specimens detailing configurations.

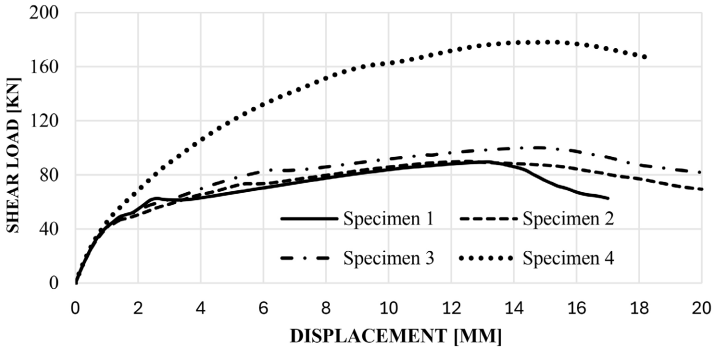

Figure 9. Load-displacement curves obtained for specimens from numerical analysis.

3.1. Specimen 1

Figure 9 compares the load-displacement curves of all the specimens under review. All the specimens exhibit the same stiffness until a 1 mm displacement at a load of 41 kN, because all the load (at this stage) was carried by the concrete alone. Beyond this stage, specifically a 2 mm displacement, which corresponds to 54.7 kN, the stiffness has reduced slightly due to the formation of cracks directly beneath the applied load. The first peak load was recorded at a displacement of 2.6 mm with a shear load of 62.6 kN. After the peak load, concrete's contribution to the load capacity of specimen 1 begins to drop, and the reinforcement contribution increases through intercepted cracks. The maximum load capacity of 89.6 kN at 13.2 mm is reached through a steady rise in the load-displacement graph. Beyond the second peak load, an abrupt drop in the curve was observed.

Figure 10(a) and Figure 10(b) are crack patterns obtained at the first and second peak loads for specimen 1, respectively, while Figure 10(c) and Figure 10(d) show the corresponding tensile stresses along the longitudinal rebar, just at 595 MPa (Tensile strength of the rebar). The failure cracks originate from the connection between the tread and riser, spreading horizontally through the risers and at an angle of approximately 45 degrees through the treads. This crack pattern is very similar to the Type-z detailing configuration obtained in the experimental test by Özbek *et al.* [4]. The failure mode appears to be a concrete breakout at the tread and riser of the section. This failure mode arises early in the analysis due to the absence of confined closed-loop stirrups at the tread-riser joint panel. Figure 10(e) shows a weak strut (principal compressive stresses) formation along the length of the staircase, which is due to the unavailable closed-loop shear reinforcement (shear links) around the tead-riser joints. This map also relates to the direction of the principal tensile stresses, which are perpendicular to the principal compressive stresses being displayed.

3.2. Specimen 2

Specimen 2's load-displacement curve behavior is similar to that of Specimen 1, with the exception that there was no first peak load developed until the failure load of 90 kN at 12.6 mm displacement. Beyond this stage, the graph descends gradually.

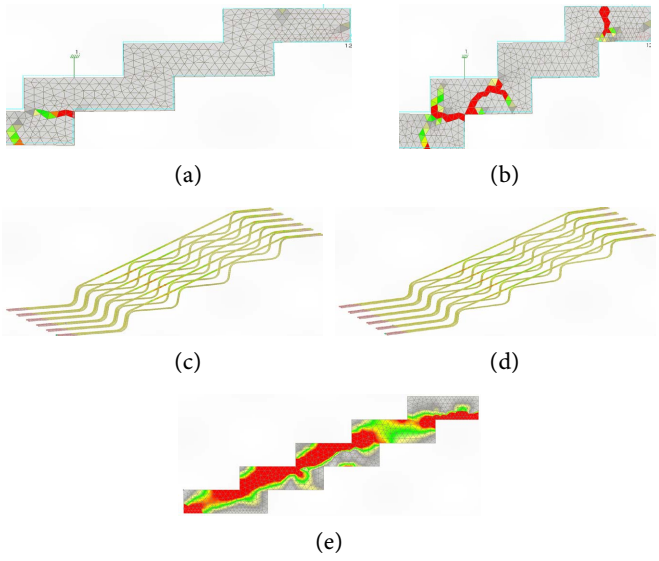

Figure 10. Crack pattern obtained from numerical analysis for Specimen 1 (a) at peak load, and (b) at 2nd peak load. Von Mises steel stresses along the rebar (c) at the 2nd peak, and at (d) the 2nd post-peak load. (e) Principal compressive stresses along the stairs at the 2nd post peak.

Figure 11(a) and Figure 11(b) show the crack propagation at the peak and post-peak phase of specimen 2, which is similar to the crack formation developed in specimen 1. Flexural cracks were also observed at the lower tread of the stairs. The steel stresses recorded (approximately 250 MPa) in the rebars did not reach the 595 MPa yield stress (Figure 11(c) and Figure 11(d)). The failure mode appears to be a concrete breakout at the tread and riser of the section, resulting from the absence of shear links at the tread-riser joint, similar to that observed in specimen 1.

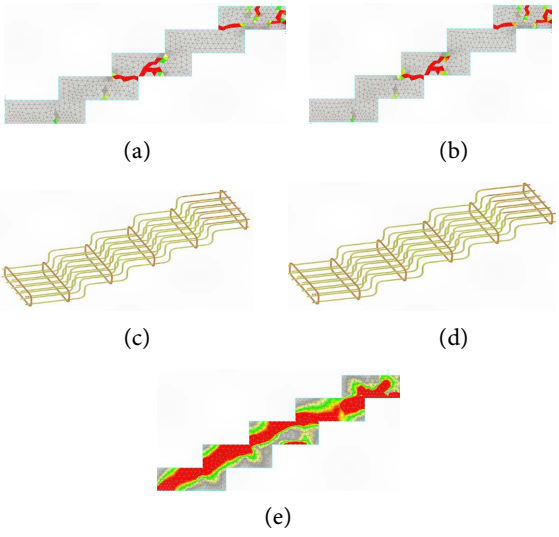

Figure 11. Crack pattern obtained from numerical analysis for Specimen 2 (a) at peak load, and (b) at post-peak load. Von Mises steel stresses along the rebar (c) at the 2nd peak, and at (d) post-peak load. (e) Principal compressive stresses along the stairs at peak load.

Figure 11(e) maps the weak strut (principal compressive stresses) developed along the length of the staircase, although spread across the cross-section, compared to specimen 1 at peak load. However, the absence of confined closed links reduces its width.

3.3. Specimen 3

The installation of an extra transverse steel loop in each tread of the slabless stairs in specimen 3, as compared to specimen 2, resulted in an increased failure load of 100 kN, at a displacement of 14.8 mm. Consequently, the graph behavior resembles that observed with specimen 2. As a result, with crack patterns and principal compressive stress distribution are similar to specimen 2.

3.4. Specimen 4

Specimen 4 had closed loops of rebars (forming a rigid, chain-like zigzag frame) along the length of the slabless staircase. The graph showed a significant improvement in stiffness compared to other specimens under review. It is also important to note that the system demonstrated its ability to dissipate a large amount of energy, as indicated by the area covered by the load-displacement curve shown in Figure 9. The shear load vs displacement curve exhibited ductile behavior, as it maintained its failure load of 178 KN at a displacement of 15.2 mm over a period of time. Beyond this stage is a gradual drop in the curve.

Crack propagation in Figure 12(a) and Figure 12(b) shows fully developed flexural cracks and concrete crack breakout in the treads and risers. Interestingly, the crack formations are in tandem with similar rebar arrangements of Type-t, as observed in the experimental results of Özbek *et al.* [4]. Arguably, the ductile behavior of the graph is due to the ability of significant portions of the rebars to attain tensile yield stresses, as shown in Figure 12(c) and Figure 12(d). Consequently, the failure mode appears to be a combination of concrete breakout at the tread and riser of the section, as well as yielding of the rebars. Figure 12(e) illustrates a more pronounced formation of principal compressive stresses compared to other specimens under review. The installation of shear links around the tread-riser joints ensured the formation of stable struts in the system. As a result of the stable strut formation within the closed loops of the rebars, the load-carrying capacity of the system is further enhanced.

4. Comparison of Numerical Shear Loads with Allowable Loads

This section compares the shear loads of all the specimens under review with the ultimate allowable loads specified in the relevant codes [6]-[8]. Table 3 summarises the mean shear loads in kN and the corresponding design area loads in kN/m^2. In this Table, $F_{\max}$ is the failure load from the numerical analysis of all the specimens. While $V_n = 0.6F_{\max}$ is the corresponding shear resistance in kN/m^2.

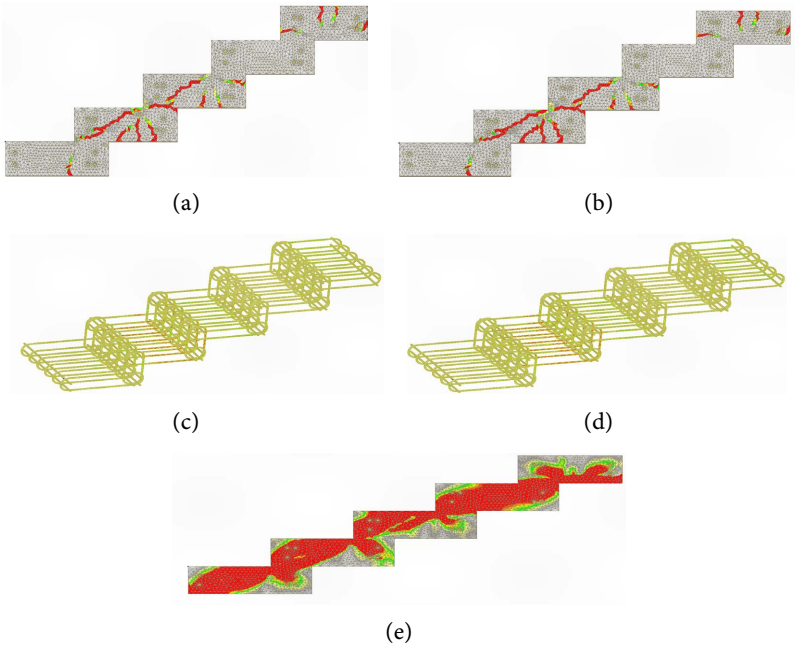

Figure 12. Crack pattern obtained from numerical analysis for Specimen 4 (a) at peak load, and (b) at post-peak load. Von Mises steel stresses along the rebar (c) at the 2nd peak, and at (d) post-peak load. (e) Principal compressive stresses along the stairs at peak load.

Table 3. Failure load comparison to the Numerical test.

	F_{max}	F_{max}	F_{max}	V_n	Relative increase in load
Specimen	[kN]	[kNm/0.6m]	[kN/m^2]	[kN/m^2]	$\frac{V_n}{\text{ULC}}$
1	89.6	39.96	61.60	36.96	2.19
2	90	37.12	61.87	37.125	2.20
3	100	41.25	68.75	41.25	2.44
4	178	73.42	122.38	73.425	4.34

The ultimate allowable load of the staircase will be computed by the combination of the self-weight of the slabless staircase derived in Equation (4.1), additional deadload (finishes) of 1.2 kN/m^2 and live load of stairs for school from [7], 4.79 kN/m^2

$$\text{Self-weight} = \frac{\left(\text{Tread width} \times \text{Tread Thickness} + \text{Riser} \times \text{Riser Thickness}\right) \times 24\ \text{kN/m}^3}{\text{Tread width}} \quad (4.1)$$

$$\text{Self-weight} = \frac{\left(0.3\ \text{m} \times 0.15\ \text{m} + 0.15\ \text{m} \times 0.15\ \text{m}\right) \times 24\ \text{kN/m}^3}{0.3\ \text{m}} = 5.4\ \text{kN/m}^2$$

Using the ultimate load combination (ULC) for strength from [7], the maximum factored load is 16.9 kN/m^2. The relative increase in load of all the specimens is above 200% when compared to the ULC of a school staircase. Only specimen 4

has a 434% increase in capacity (see Table 3).

Considering that all specimens produced a relative increase of over 200%, these results suggest that all the detailing practices discussed in this paper are sufficient for detailing a slabless staircase in a non-seismic zone as observed from the behavior of their load-displacement response. Conversely, only specimen 4 is suitable for a seismic region because the rebar configuration ensured enhanced confinement of the tread-riser joint panel, resulting in ductile performance of the curve.

5. Conclusions

In this paper, a numerical study on the detailing practice of a straight flight slabless staircase under monotonic displacement control at the mid-span of the specimens has been investigated. The purpose was to examine the behavior of the discussed detailing practices in terms of their failure mode, crack pattern, and stress flow in concrete. The following major conclusions could be drawn from this work:

1) All four (4 nos) detailing specimens are appropriate for a slabless staircase since their relative increase in load when compared to the ULC of a school staircase was greater than 200%.

2) Specimen 4, with closed loops of rebars, exhibited a better performance in terms of the ductile behavior of the load-displacement curve due to its ability to ensure significant yielding of its main rebars and also the formation of stable struts.

3) The failure mode exhibited by specimens 1, 2, and 3 is a brittle concrete breakout at the tread and riser section.

4) Detailing practice of specimen 4 requires greater tonnage(s) of rebars and complexity in rebar installation compared to specimens 1 - 3. Consequently, there is an increase in construction costs.

Note

The conclusions given above are due to the FE analysis on the four detailing specimens discussed in this work. Other detailing practices that have planar longitudinal rebar with closed loops or rebars were not addressed. Furthermore, experimental investigations are needed to verify the findings in this work.

Conflicts of Interest

The author declares no conflicts of interest regarding the publication of this paper.

References

[1] Jiang, R.J. and Au, F.T.K. (2011) A General Finite Strip for the Static and Dynamic Analyses of Folded Plates. *Thin-Walled Structures*, **49**, 1288-1294. https://doi.org/10.1016/j.tws.2011.05.006

[2] Saenz, L.P. and Martin, I. (1961) Slabless Tread-Riser Stairs. *ACI Journal Proceedings*, **58**, 353-366.

[3] Cusens, A.R. (1966) Analysis of Slab-Less Stairs. *Concrete and Constructional Engineering*, **61**, 359-364.

[4] Özbek, E., Kaya, Y., Bocek, M. and Aykaç, S. (2021) Flexural Behavior of Slabless Rein-forced Concrete Staircases. *ACI Structural Journal*, **118**, 63-73.

[5] Sabeeh, R.S. and Jaafer, A.A. (2024) Slabless Staircase Flexural Behavior with Multi Reinforcement Configuration. *Misan Journal of Engineering Sciences*, **3**, 167-181.

[6] (2019) ACI 318. Building Code Requirements for Structural Concrete (ACI 318-19) and Commentary (ACI 318R-19). American Concrete Institute. https://www.concrete.org/Portals/0/Files/PDF/Previews/318-19_preview.pdf

[7] (2020) ASCE 7-16. Guide to the Seismic Load Provisions. American Society of Civil Engineers. https://ascelibrary.org/doi/book/10.1061/9780784415504

[8] (2018) EN 1992-4. Eurocode 2: Design of Concrete Structures-Part 4: Design of Fastenings for Use in Concrete. European Committee for Standardization (CEN). https://www.phd.eng.br/wp-content/uploads/2015/12/en.1992.1.1.2004.pdf

[9] Ožbolt, J., Li, Y. and Kožar, I. (2001) Microplane Model for Concrete with Relaxed Kinematic Constraint. *International Journal of Solids and Structures*, **38**, 2683-2711. https://doi.org/10.1016/s0020-7683(00)00177-3

[10] Lachinger, S. and Bergmeister, K. (2014) Randnahe Mehrfachbefestigungen unter kombinierter Belastung. *Beton- und Stahlbetonbau*, **109**, 334-343. https://doi.org/10.1002/best.201300091

[11] Tonidis, M. (2018) Behaviour of Lap Splices under Fire. Master's Thesis, University of Stuttgart.

[12] Oyakojo, E. (2023) Numerical Investigations on Bonded Anchors with Post-Installed Supplementary Reinforcement Under Tension Loading. Master's Thesis, Purdue University.

[13] Bhattachan, A. (2025) Numerical Study on Non-Seismically Designed RC Interior Beam-Column Joints Fastened Haunch Retrofit Solution. Master's Thesis, Purdue University.

[14] Rehman, M. (2022) Numerical Investigation of Closely Spaced Anchor Groups Under Different Geometric and Loading Conditions. Master's Thesis, Purdue University.

[15] Appa Rao, G. and Kadhiravan, D. (2013) Nonlinear FE Modelling of Anchorage Bond in Reinforced Concrete. *International Journal of Research in Engineering and Technology*, **2**, 377-385.

[16] Bokor, B. and Sharma, A. (2021) Numerical Investigations on Non-Rectangular Anchor Groups under Shear Loads Applied Perpendicular or Parallel to an Edge. *CivilEng*, **2**, 692-711. https://doi.org/10.3390/civileng2030038

[17] Karihaloo, B.L. (1995) Fracture Mechanics and Structural Concrete. Longman Scientific and Technical Publishers. https://www.scribd.com/document/387273194/B-L-Karihaloo-Fracture-Mechanics-and-Structural-Concrete-pdf